AIP | Advances

Estimation of the temperature dependent interaction between uncharged point defects in Si

Eiji Kamiyama, Jan Vanhellemont, and Koji Sueoka

Citation: AIP Advances **5**, 017127 (2015); doi: 10.1063/1.4906565
View online: http://dx.doi.org/10.1063/1.4906565
View Table of Contents: http://scitation.aip.org/content/aip/journal/adva/5/1?ver=pdfcov
Published by the AIP Publishing

AIP ADVANCES **5**, 017127 (2015)

Estimation of the temperature dependent interaction between uncharged point defects in Si

Eiji Kamiyama,[1,2,a] Jan Vanhellemont,[3] and Koji Sueoka[1]
[1]*Department of Communication Engineering, Okayama Prefectural University, 111 Kuboki, Soja-shi, Okayama-ken 719-1197, Japan*
[2]*GlobalWafers Japan Co., Ltd., 30 Soya, Hadano, Kanagawa, 257-8566, Japan*
[3]*Department of Solid State Sciences, Ghent University, Krijgslaan 281-S1, Ghent B-9000, Belgium*

(Received 2 July 2014; accepted 13 January 2015; published online 22 January 2015)

A method is described to estimate the temperature dependent interaction between two uncharged point defects in Si based on DFT calculations. As an illustration, the formation of the uncharged di-vacancy V_2 is discussed, based on the temperature dependent attractive field between both vacancies. For that purpose, all irreducible configurations of two uncharged vacancies are determined, each with their weight given by the number of equivalent configurations. Using a standard 216-atoms super-cell, nineteen irreducible configurations of two vacancies are obtained. The binding energies of all these configurations are calculated. Each vacancy is surrounded by several attractive sites for another vacancy. The obtained temperature dependent of total volume of these attractive sites has a radius that is closely related with the capture radius for the formation of a di-vacancy that is used in continuum theory. The presented methodology can in principle also be applied to estimate the capture radius for pair formation of any type of point defects. [http://dx.doi.org/10.1063/1.4906565]

I. INTRODUCTION

Silicon crystals grown by the Czochralski technique can contain voids leading to so-called crystal originated pits (COP's) on polished wafer surfaces. These voids that are also observed in Czochralski-grown germanium crystals, are large vacancy clusters that are formed during cooling immediately after solidification.[1] COP's have a detrimental impact on gate oxide integrity and can cause also problems with epitaxial layer quality.[2–4] Besides intrinsic point defect pairs and clusters, also a wide variety of impurity-intrinsic point defect pairs and clusters are known.[5] In continuum theory, point defect pair formation kinetics are described by rate equations, assuming a temperature independent capture radius.[6] The capture radius that is used in these rate equations, is mostly chosen arbitrarily in order to have a good agreement with experimental results. Furthermore, isotropic diffusion is mostly assumed in the theory of diffusion-limited reactions of reacting point defects in a solid,[6] while in real crystals the point defect diffusivity depends on the crystallographic directions.

The reaction rate k_f for the formation of a point defect pair AB, is commonly written as:

$$k_f = 4\pi r(D_A + D_B) \tag{1}$$

where r is the capture radius of point defect A and B and D_A and D_B are the diffusion coefficients of A and B, respectively. The capture radius is usually assumed to be of the order of the bond length of Si with values depending on the type of point defect pair.[7–10] 0.5 nm is a value that is typically used to describe the formation kinetics of the di-vacancy.[7,10]

[a]ejkamiyama@aol.com

In the past, material related phenomena have mostly been described using continuum models with empirical model parameters, due to a lack of atomistic models and calculation methods. Nowadays, ab initio calculations can be used to reveal the atomistic details and processes behind the continuum models. In a previous paper,[11] an atomistic picture of the diffusion of two uncharged vacancies forming a di-vacancy in Si was discussed, based on DFT calculations using 64-atoms supercells. Due to the 64 atoms supercell, it was not possible to investigate sufficiently accurate the long-range interaction between the two vacancies which is needed for the determination of the interaction volume between the two point defects.

In the present paper, the interaction of two vacancies is investigated by using a 216-atoms supercell for the DFT calculations, which allows calculating with high accuracy the temperature dependent radius of the attractive field surrounding the vacancy which is a good and non-empirical approximation of the capture radius used in continuum theory.

II. CALCULATION DETAILS

A. Irreducible point defect pair configurations

A program code was used allowing determining all basic irreducible atomic configurations of two vacancies in the 216-atoms supercell. The weight of each configuration is determined as the number of equivalent configurations and this is done by considering the symmetry of the Si crystal and the periodic condition of the supercell. This search is performed automatically by using a script program code based on a published algorithm,[12] and is similar to a method used elsewhere.[13] All the atomistic models are automatically produced, not including the local distortions although there is of course an influence of the initial local distortion of the position of atoms around the vacancies due to the Jan-Teller effect.[14] The local distortions are neglected as they have only a small effect on the calculated interaction volume around the vacancy. The main goal of the present paper is indeed not a detailed study of the silicon di-vacancy but rather to illustrate an approach that can be used for all types of point defect pairs. When studying more in detail a specific point defect pair, such details can be taken into account in the ab initio calculations whenever considered useful.

It turns out that there are nineteen irreducible configurations of two vacancies in the 216-atoms cell while in a 64-atoms cell there are only nine.[11] These configurations have been automatically extracted from the total numbers of 23220 ($= {}_{216}C_2$) possible configurations for a 216-atoms supercell. In some of these configurations, two vacancies are on a same zigzag bond along a <110> direction in a {110} plane and have a stronger interaction similar as between the vacancy and an impurity atom.[15]

B. DFT calculation procedure

The DFT calculations are based on the standard approach, using the local density approximation[16,17] with the ultrasoft pseudopotential method,[18] and plane waves as basis set for efficient structure optimization. The generalized gradient approximation (GGA) is used for describing the exchange–correlation energy, in the Perdew–Burke–Ernzerhof (PBE) form.[19] The *CASTEP* code is used to self-consistently solve the Kohn-Sham equation using a three-dimensional periodic boundary condition.[20] The density mixing method[21] and the BFGS geometry optimization method[22] are used to optimize the electronic structure and the atomic configurations, respectively. Only the neutral charge state of the system, which corresponds to vacancies introduced in nearly intrinsic Si, is considered in the present study. Even in more heavily doped Si this is a useful approximation in the early stage of cooling after solidification during Si single crystal growth from a melt. For k-point sampling, the $2 \times 2 \times 2$ special points of the Monkhorst-Pack grid[23] are used. The cutoff energy of the plane waves is 350 eV. Under these conditions, the supercell of the perfect Si was optimized and is a cube with a 1.639 nm size. Each cell with these nineteen basic configurations of two vacancies is then created and relaxed fully. Furthermore, the binding energy of the two vacancies is calculated for each configuration by using the formation energy of an uncharged isolated V which is 3.58 eV for a 216-atoms supercell as calculated by the standard approach based on the Si atom self-energy in

the perfect cell. Although the energy differences between this size cell and 64 atoms cell[11] is about 0.3 eV for the second vacancy at positions #1 or #3, the sites at a distance in the range 0.6-0.8 nm, except site #6, #9 which are on the cell boundary in a 64 atom cell, have converged to values differing less than 0.1 eV from those obtained with the 216 atom supercell.

III. RESULTS AND DISCUSSION

A. Binding energy between two vacancies

Fig. 1(a) shows the relative configuration of two vacancies whereby one vacancy is approaching the second one which is assumed to be fixed at the position labeled #0 in Fig. 1(a). Figure 1(b) shows the binding energies of the nineteen basic configurations of two vacancies in a 216-atoms supercell as a function of the nominal distance between them. The different vacancy positions in Fig. 1(b) are labeled by the numbers corresponding to the numbers in Fig. 1(a). In Fig. 1(b), each V position is defined by the position of the Si atom before forming V and before structural relaxation. The most stable configuration is labeled #1. This configuration describes two vacancies located at the nearest neighbor site, i.e., the di-vacancy. The obtained binding energy E_b is 1.75 eV, significantly higher than the 1.43 eV obtained before for a 64-atoms supercell.[11] Both values are lower than the calculated 2 eV reported in literature[24,25] but are close to the reported experimental values of 1.5 eV[26] and $\gtrsim$1.6 eV.[27] The second V set at position #2 as an initial model of the atoms in 216-atoms cell moved to the #1 position (forming a di-vacancy) after the geometry optimization. There was a meta-stable position for the second V at #2 and no trasition state was found between #1 and #2 positions for the second V in 64-atoms cell.[11] The 216-atoms cell size is large enough to estimate the attractive volume size since the binding energy of the second V at #9 become negative thus limiting the number of binding sites. Comparing to the 64-atoms supercell, the binding energies of the second V at #3~6 or #7-1 increased.

B. Repulsion and attraction between two vacancies

Figure 1(a) shows the binding energies between one V fixed at the position #0 and a second V which is mobile. The fixed V is surrounded by attractive sites (blue or light blue circles), and by repulsive sites (red or light red circles). In some configurations like #0-#7-2, #0-#13 and #0-#18, as shown in Fig. 2, the two vacancies have a negative binding energy smaller than -0.45 eV. It is interesting to note that configurations #7-1 and #7-2 have the same distance between the two vacancies but have totally different binding energies. Since the sites that have a negative binding energy (= are repulsive) are limited in number, the effect of these sites is ignored in the following when estimating the attractive interaction volume around a vacancy. A second vacancy at a site with negative binding energy will indeed move to a neighboring site with a positive binding energy.

C. The impact of the attractive and repulsive fields on vacancy pairing

An isolated V has a migration energy of about 0.25 eV.[28] When this moving V enters the interaction volume of another vacancy with several attractive sites (blue or light blue circles in Fig. 1(a)), the moving vacancy will slow down by being temporarily trapped in sites with low binding energy. When the trapped vacancies are released again, they will preferentially move to sites with larger binding energy and finally end up in the most stable configuration being the well-known di-vacancy. The range of the attractive field surrounding a vacancy, is therefore closely related to the capture cross-section or capture radius used in continuum modeling. The volume of this field (which is not spherical due to its dependence on crystallographic directions) can be converted into an attractive field radius, which is an approximation of the capture radius by averaging as discussed further below. In a previous paper,[11] a first estimation of this volume was obtained using a 64-atom supercell which is however too small to contain to complete attractive volume for which an at least 216-atoms supercell (4.40 nm^3).

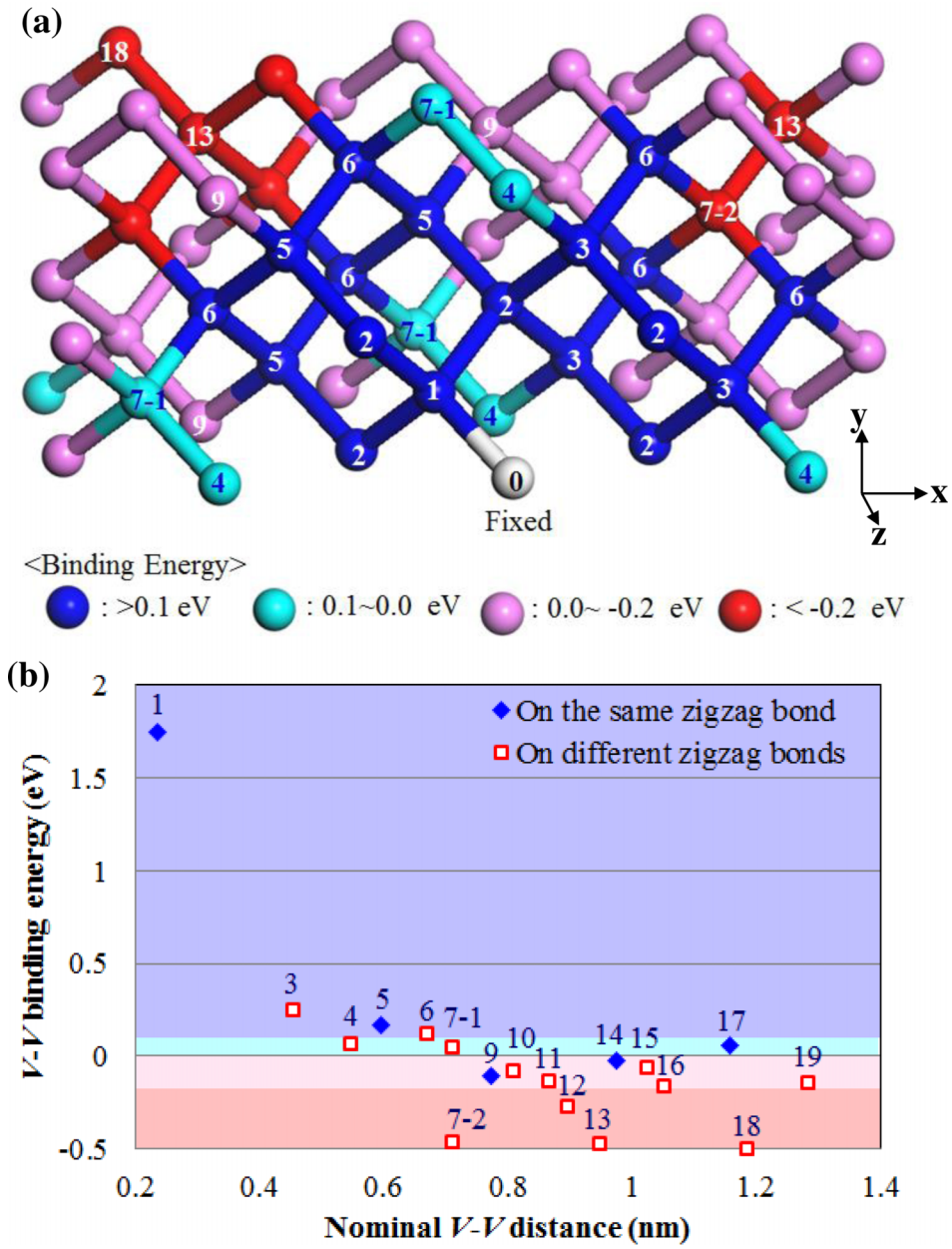

FIG. 1. (a) Configurations of two vacancies in a 216-atoms supercell supposing one vacancy is fixed at #0 while the other one can migrate, (b) Binding energies as a function of the nominal distance for the basic configurations of two vacancies in a 216-atoms supercell, whereby one vacancy is assumed to be immobile. The color zones correspond with the colors used in (a). The second V set at position #2 in the initial model of the atoms in 216-atoms cell moved to the #1 position (forming a di-vacancy) after the geometry optimization and therefore there is no #2 in the figure. The filled diamonds are the energies of the second V on the same zigzag bond as the fixed vacancy. The open squares are the energies of the second V on a zigzag bond different from the fixed vacancy.

D. The attractive field at 0 K

The extent of the attractive field around vacancy for a second vacancy is determined by the $E_b>0$ sites listed in Table I. Table II shows that when assuming $0 = <E_b<E_{b1}$, all sites except #17 can contribute to the attractive field surrounding site #0. The ratio of the volume of the attractive field and the volume of the supercell is estimated by calculating the ratio of the summed weights of the attractive sites and the total number of sites in the supercell. Hereby the relaxations of atoms

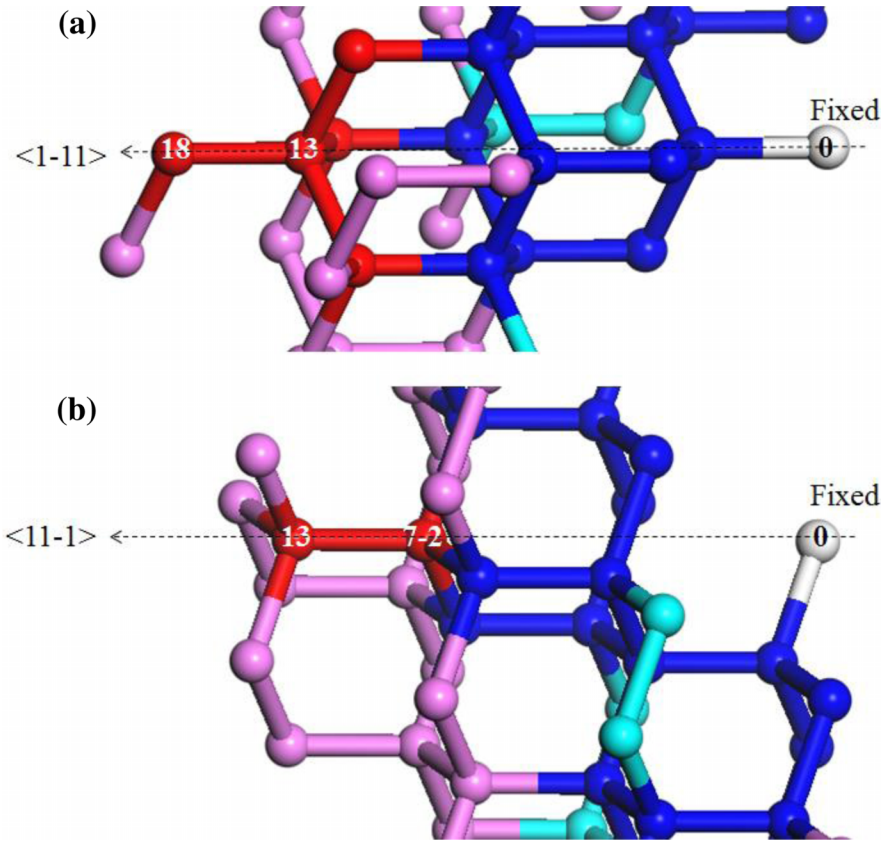

FIG. 2. Configurations of two vacancies with a negative binding energy smaller than -0.45 eV: (a) #0-#13 and #0-#18, (b) #0-#7-2. For those configurations, the vacancies are aligned along the <111> directions.

around the vacancies are neglected after the relaxation calculations. Using criterion (a) of Table II, yields a radius r of the attractive field at 0 K of 0.74 nm. Using the criteria (b) or (c) of Table II to define the radius of the attractive field, yields values of 0.70 and 0.68 nm, respectively. This gives an idea of the uncertainty on r, depending the criterion one uses to define the boundary of the attractive field.

E. The temperature dependent attractive field

With increasing temperature, dissociation of the pair of point defects into two separate point defects will become more and more important. In continuum theory, the reaction rate k_r of this

TABLE I. Sites with positive binding energy E_{bi}.

Site#	Symbol E_{bi}	E_b (eV)
1	E_{b6}	1.75
2	E_{b6}	(1.75)[a]
3	E_{b5}	0.25
5	E_{b4}	0.16
6	E_{b3}	0.12
4	E_{b2}	0.073
7-1 / 17	E_{b1}	$\approx$ 0.055[b]

[a]The second V moved to the #1 position (forming a di-vacancy) after the geometry optimization.
[b]Values are very close to each other.

TABLE II. Maximum separation of two vacancies, estimated based on weight (= the number of equivalent configurations), attractive interaction and site geometry for all irreducible configurations in a 216-atoms supercell. Starting from position 7-2 of the second vacancy, the binding energy E_b, arising from the interaction with the fixed V at site #0, becomes negative.

			(a)		(b)		(c)		(d)		(e)		(f)		(g)	
			$0 =< E_b < E_{b1}$		$E_{b1} =< E_b < E_{b2}$		$E_{b2} =< E_b < E_{b3}$		$E_{b3} =< E_b < E_{b4}$		$E_{b4} =< E_b < E_{b5}$		$E_{b5} =< E_b < E_{b6}$		$E_{b6} < E_b$	
Second V site #	weight (23436 total)	Binding energy E_b^i (eV)	Attractive ?	Connected to site #0 ?	Attractive ?	Connected to site #0 ?	Attractive ?	Connected to site #0 ?	Attractive ?	Connected to site #0 ?	Attractive ?	Connected to site #0 ?	Attractive ?	Connected to site #0 ?	Attractive ?	Connected to site #0 ?
0	216	-	(core)	Y	(core)	Y	(core)	Y	(core)	Y	(core)	Y	(core)	Y	(core)	Y
1	432	1.75	Y	Y	Y	Y	Y	Y	Y	Y	Y	Y	Y	Y	Y	Y
2	1296	(1.75)	Y	Y	Y	Y	Y	Y	Y	Y	Y	Y	Y	Y	N	N
3	1296	0.25	Y	Y	Y	Y	Y	Y	Y	Y	Y	Y	N	N	N	N
4	648	0.07	Y	Y	Y	Y	N	N	N	N	N	N	N	N	N	N
5	1296	0.16	Y	Y	Y	Y	Y	Y	Y	Y	N	N	N	N	N	N
6	2592	0.12	Y	Y	Y	Y	Y	Y	N	N	N	N	N	N	N	N
7-1	1296	0.06	Y	Y	N	N	N	N	N	N	N	N	N	N	N	N
7-2	432	-0.46	N	N	N	N	N	N	N	N	N	N	N	N	N	N
9	1296	-0.10	N	N	N	N	N	N	N	N	N	N	N	N	N	N
10	2592	-0.08	N	N	N	N	N	N	N	N	N	N	N	N	N	N
11	1296	-0.13	N	N	N	N	N	N	N	N	N	N	N	N	N	N
12	1296	-0.27	N	N	N	N	N	N	N	N	N	N	N	N	N	N
13	864	-0.47	N	N	N	N	N	N	N	N	N	N	N	N	N	N
14	1296	-0.03	N	N	N	N	N	N	N	N	N	N	N	N	N	N
15	2592	-0.06	N	N	N	N	N	N	N	N	N	N	N	N	N	N
16	1296	-0.16	N	N	N	N	N	N	N	N	N	N	N	N	N	N
17	324	0.06	Y	N	N	N	N	N	N	N	N	N	N	N	N	N
18	432	-0.50	N	N	N	N	N	N	N	N	N	N	N	N	N	N
19	648	-0.18	N	N	N	N	N	N	N	N	N	N	N	N	N	N
Attractive & connected to #0			9072		7776		7128		4536		3240		1944		648	
Volume of attractive field (nm^3)			1.71		1.46		1.34		0.85		0.61		0.37		0.12	
Maximum separation r_i (nm)			0.74		0.70		0.68		0.59		0.53		0.44		0.31	

reverse pairing or dissociation reaction is expressed as:

$$k_r = k_f C_A C_B / C_{AB} \tag{2}$$

k_f is the reaction rate of the pairing process, while C_A, C_B, C_{AB} are the concentrations of the point defects A, B and of the point defect pair AB, respectively. In the atomistic picture of the migration of the second V, the pairing and dissociation reactions always occur successively with the probability of both reactions determined by the activation energy of the point defect for the migration. Both reactions can be described by probabilities, which have to be introduced into the concept of the interaction field in the atomistic picture.

Therefore, in this paper, the interaction field is determined using the capture probability p of the second mobile V by the fixed one at #0, having a binding energy E_b. This binding energy is defined with respect to the energy of the two vacancies at infinite distance from each other. Figure 3 shows schematically the relation between p_i and E_{bi} assuming an activation energy E_{ai} for diffusion of the second V at the site with binding energy E_{bi}. Here, this activation energy E_{ai} takes into account all barriers, including the repulsive sites around the attractive sites in Fig. 1(a), for the second V to diffuse from infinity to the site with a binding energy E_{bi}. Assuming that the vacancy concentration, which can be applied for eq. (2), around the barriers is uniform, the prefactors describing the inbound and out bound diffusion can be assumed to be the same and the capture probability p_i can be written as 1-exp[-E_{bi}/k_BT]. When the temperature T approaches to 0 K, p_i becomes 1 (100%) in case of $E_{bi} > 0$ as discussed above. The capture probability p_i on the site with binding energy E_{bi} depends on the binding energy E_{bi} in Table I as p_i = 1-exp[-E_{bi}/k_BT]. Figure 4(a) shows the p_i dependences on T for sites having each binding energy E_{bi}, which classified the nominal capture radius r_i in Table II. The reaction rate k in eq.(1) would be over-estimated when using r_i. This is because r_i is deduced under the condition $p_i < 1$. To avoid this problem, we evaluated r in eq. (1) as $p_i r_i$. Figure 4(b) shows the calculated $p_i r_i$ for each binding energy E_{bi} (i.e., each second V site) in Fig. 4(a). As we consider all p_i, $p_i r_i$ has a different value for each p_i at each temperature. With increasing temperature, all p_i decrease and lead to lower $p_i r_i$. When $p_i r_i$ starts to decrease, $p_{i+1} r_{i+1}$ is larger than $p_i r_i$. This means that with increasing temperature, the second vacancy will be captured at sites closer to the first vacancy and will form a vacancy pair there with high probability due to the higher binding energy as shown in Fig. 4(b). Therefore, the black curve, which is the maximum of these values for each temperature in Fig. 4(b), is the most probable radius of the effective attractive field and a good approximation for r in eq. (1). It may, however, be an overestimate considering all other possible geometries of the second vacancy after the p_i process mentioned above. The real value of the radius is therefore expected to lie between the curves corresponding with the maximum and the averaged r values, also shown in Fig. 4(b).

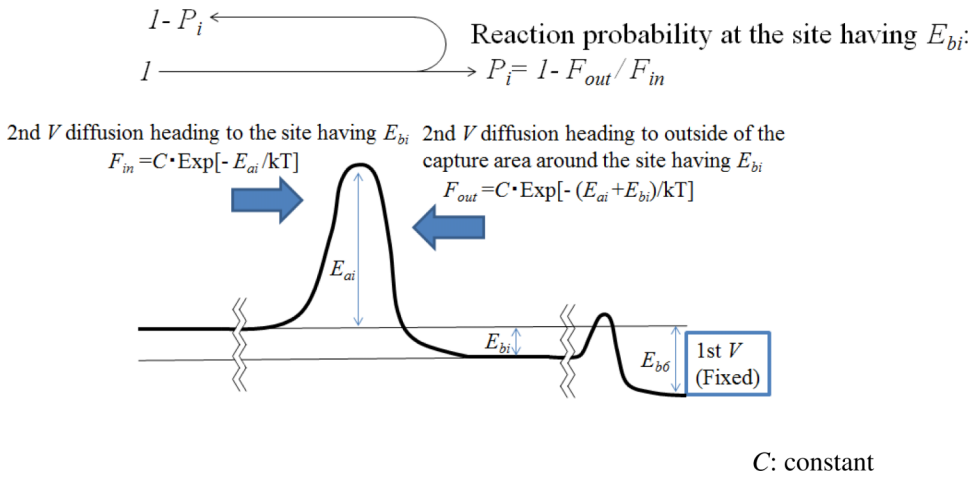

FIG. 3. Schematic representation of the relation between p_i and E_{bi} at the site with binding energy E_{bi} around the capture radius from the fixed V at the site #0 with an activation energy E_{ai} of the migration for the second V.

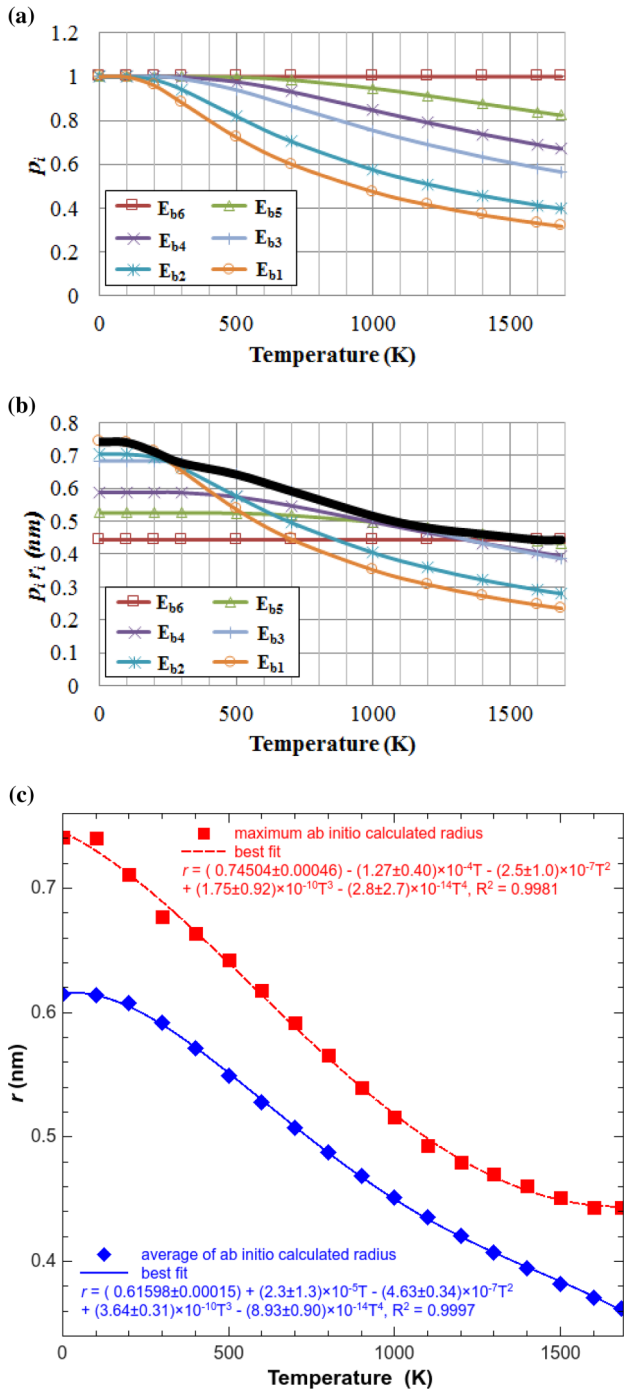

FIG. 4. (a) Dependence on the temperature of the probabilities p to form a di-vacancy for each criterion for the binding energy E_{bi}, which is given in Table I, (b) Dependence on the temperature of $p_i r_i$, which can be used as the capture radius r in eq. (1), converted from data in (a). The black line shows the dependence on the temperature of the maximum of $p_i r_i$. (c) Best polynomial fit to the black line in (b) of ab initio capture radius r_{att} between 0 K and the melting temperature (1685 K). The best polynomial fit to the average of $p_i r_i$ in (b) is also included for comparison.

The radius of the attractive field is nearly constant at temperatures below 100 K. At these low temperatures, the thermal energy becomes so small that it drops below the 0.1 eV that we assumed as a kind of cut off energy due to the inaccuracy of the ab initio calculation. This leads to an apparent constant radius.

A fourth order polynomial fit ($R^2 = 0.998$) of the initio calculated values of the attractive field radius r_{att} corresponding with the maximum $p_i r_i$ values between 0 K and melting temperature is shown in Fig. 4(c). The thus obtained polynomial fit

$$r_{att}(T) = (0.7450\pm0.0005) - (1.27\pm0.40) \times 10^{-4}T - (2.5\pm1.0) \times 10^{-7}T^2 + (1.75\pm0.92) \times 10^{-10}T^3 - (2.8 \pm 2.7) \times 10^{-14}T^4, \quad (3)$$

can in first order approximation replace r in Eq. (1) between 0 K and melting temperature. Eq. (3) yields a value of 0.69 nm at room temperature, which is close to the capture radius for a di-vacancy used in the continuum models. The ab initio approach has the advantage that is based on an atomistic model, without making empirical choices. Furthermore it describes the temperature dependence of r which should allow more accurate modeling of rate equations.

As illustrated in Fig. 1(b), the attractive field for the second V contains also repulsive sites, in which some sites even have a negative binding energy smaller than -0.45 eV depending on the crystallographic directions around the fixed V. The presented methodology can in principle also be applied for calculating the interaction field leading to pair formation of any type of point defects, also those that have a longer interacting range than the 0.6 nm for V_2 formation[29,30] in which case also a larger supercell should be used for the calculations. Longer interaction ranges will in most cases also lead to larger capture radii.

IV. CONCLUSIONS

A method is proposed to estimate the radius of the interaction field for the formation of a point defect pair in Si based on an atomistic picture. This radius is closely related to the capture radius used in continuum theory. The application of the method is illustrated by the simplest case which is the formation of a di-vacancy by pairing of two uncharged vacancies. Describing the point defect association and dissociation reactions by probabilities, the temperature dependence of the radius r of the interaction field can be obtained showing that it gradually decreases as the temperature increases as should therefore also be the case for the capture radius in the continuum model.

ACKNOWLEDGMENT

This work is partially supported by the Advanced Low Carbon Technology Research and Development Program (ALCA) of the Japan Science and Technology Agency (JST). We are also indebted to Dr. Abhijit Chatterjee of Accelrys Software Inc., for stimulating discussions and for developing the script program code that is used in the present study to calculate the irreducible vacancy configurations.

[1] J. Vanhellemont and E. Simoen, J. Electrochem. Soc. **154**, H572 (2007).
[2] M. Muranaka, K. Makabe, M. Miura, H. Kato, S. Ide, H. Iwai, M. Kawamura, Y. Tadaki, M. Ishihara, and T. Kaeriyama, Jpn. J. Appl. Phys., Part 1 **37**, 1240 (1998).
[3] H. Ishii, S. Shiratake, K. Oka, K. Motonami, T. Koyama, and J. Izumitani, Jpn. J. Appl. Phys., Part 2 **35**, L1385 (1996).
[4] M. Miyazaki, S. Miyazaki, T. Kitamura, Y. Yanase, T. Ochiai, and H. Tsuya, Jpn. J. Appl. Phys., Part 1 **36**, 6187 (1997).
[5] B. Pajot and B. Clerjaud, *Optical Absorption of Impurities and Defects in Semiconducting Crystals. II. Eletronic Absorption of Deep Centers and Vibrational Spectra*, Springer Series in Solid-State Sciences (2013), Vol. 169.
[6] T. R. Waite, Phys. Rev. **107**, 463 (1957).
[7] M. Mikelsen, E. V. Monakhov, G. Alfieri, B. S. Avset, and B. G. Svensson, Phys. Rev. **B 72**, 195207 (2005).
[8] G. D. Watkins, J. Appl. Phys. **103**, 106106 (2008).
[9] H. Bracht, J. Fage Pedersen, N. Zangenberg, A. Nylandsted Larsen, E. E. Haller, G. Lulli, and M. Posselt, Phys. Rev. Lett. **91**, 245502 (2003).
[10] G. Kissinger, J. Dabrowski, and D. Kot, Jpn J. Appl. Phys. **53**, 05FJ06 (2014).
[11] E. Kamiyama, J. Vanhellemont, and K. Sueoka, Phys. Status Solidi B **251**, 2185 (2014).
[12] J. L. Gavartin, M. Sarwar, D. C. Papageorgopoulos, D. Gunn, S. Garcia, A. Perlov, A. Krzystala, D. L. Ormsby, D. Thompsett, G. Goldbeck-Wood, A. Andersen, and S. French, ECS Trans. **25**, 1335 (2009).
[13] R. Grau-Crespo, S. Hamad, C. R. A. Catlow, and N. H. de Leeuw, Journal of Physics - Condensed Matter **19**, 256201 (2007).
[14] G. Hobler and G. Kresse, Materials Science and Engineering B **124-125**, 368 (2005).
[15] K. Sueoka, E. Kamiyama, and J. Vanhellemont, J. Appl. Phys. **114**, 153510 (2013).
[16] P. Hohenberg and W. Kohn, Phys. Rev. **136**, B864 (1964).
[17] W. Kohn and L. Sham, Phys. Rev. **140**, A1133 (1965).

[18] D. Vanderbilt, Phys. Rev. **B41**, 7892 (1990).
[19] J. P. Perdew, K. Burke, and M. Ernzerhof, Phys. Rev. Lett. **77**, 3865 (1996).
[20] The *CASTEP code* is available from Accelrys Software Inc.
[21] G. Kresse and J. Furthmuller, Phys. Rev. **B54**, 11169 (1996).
[22] T. Fischer and J. Almlof, J. Phys. Chem. **96**, 9768 (1992).
[23] H. Monkhorst and J. Pack, Phys. Rev. **B13**, 5188 (1976).
[24] H. Seong and L. J. Lewis, Phys. Rev. **B 53**, 9791 (1996).
[25] D. V. Makhov and L. J. Lewis, Phys. Rev. Lett. **92**, 255504 (2004).
[26] J. W. Corbett, *Electron Radiation Damage in Semiconductors and Metals* (Academic, New York, 1996), and refs. therein.
[27] G. D. Watkins and J. W. Corbett, Phys. Rev. **138**, A543 (1965).
[28] K. Sueoka, E. Kamiyama, and H. Kariyazaki, J. Appl. Phys. **111**, 093529 (2012).
[29] K. Sueoka, E. Kamiyama, J. Vanhellemont, and K. Nakamura, Phys. Status Solidi B **251**, 2159 (2014).
[30] E. Kamiyama and K. Sueoka, J. Electrochem. Soc. **159**, H450 (2012).